Multiferroic Ni0.6Zn0.4Fe2O4-BaTiO3 nanostructures: Magnetoelectric coupling, dielectric, and fluorescence

Kuldeep Chand Verma, Sukhdeep Singh, S. K. Tripathi, and R. K. Kotnala

---

Articles you may be interested in

Superstructures of self-assembled multiferroic core-shell nanoparticles and studies on magneto-electric interactions
Appl. Phys. Lett. **105**, 072905 (2014); 10.1063/1.4893699

Physics of the multi-functionality of lanthanum ferrite ceramics
J. Appl. Phys. **115**, 204109 (2014); 10.1063/1.4879899

Magnetic field induced polarization and magnetoelectric effect of Ba0.8Ca0.2TiO3-Ni0.2Cu0.3Zn0.5Fe2O4 nanomultiferroic
J. Appl. Phys. **113**, 17C731 (2013); 10.1063/1.4795820

Magnetoelectric coupling in solution derived 3-0 type PbZr0.52Ti0.48O3:xCoFe2O4 nanocomposite films
Appl. Phys. Lett. **102**, 122905 (2013); 10.1063/1.4799174

Multiferroic behaviour of nanoporous BaTiO3
J. Appl. Phys. **110**, 064316 (2011); 10.1063/1.3641639

Multiferroic Ni$_{0.6}$Zn$_{0.4}$Fe$_2$O$_4$-BaTiO$_3$ nanostructures: Magnetoelectric coupling, dielectric, and fluorescence

Kuldeep Chand Verma,[1,2,a)] Sukhdeep Singh,[3] S. K. Tripathi,[1] and R. K. Kotnala[4]

[1]*Department of Physics, Centre of Advanced Study in Physics, Panjab University, Chandigarh 160 014, India*
[2]*Akal School of Physics, Eternal University, Baru Sahib, Himachal Pradesh 173101, India*
[3]*Akal School of Chemistry, Eternal University, Baru Sahib, Himachal Pradesh 173101, India*
[4]*National Physical Laboratory, New Delhi 110012, India*

Multiferroic nanostructures of Ni$_{0.6}$Zn$_{0.4}$Fe$_2$O$_4$-BaTiO$_3$ (NZF/BT) have been prepared by two synthesis routes, i.e., chemical combustion (CNZF/BT) and hydrothermal (HNZF/BT). The synthesis of CNZF/BT results in nanoparticles of average size 4 nm at 500 °C annealing. However, the synthesis of HNZF/BT with hydrolysis temperature 180 °C/48 h shows nanowires of diameter 3 nm and length >150 nm. A growth mechanism in the fabrication of nanoparticles and wires is given. X-ray diffraction is used to identify the crystalline phase. The transmission electron microscopy shows the dimensions of NZF/BT nanostructures. The ferromagnetism, ferroelectricity, and magnetoelectric coupling show more enhancements in HNZF/BT nanowires than CNZF/BT nanoparticles. The observed polarization depends upon shape of nanostructures, tetragonal phase, and epitaxial strain. The tension induced by the surface curvature of nanowire counteracts the near-surface depolarizing effect and meanwhile leads to unusual enhancement of polarization. The ferromagnetism depends upon superficial spin canting, spin pinning of nanocomposite, and oxygen vacancy clusters. The magnetoelectric coefficient as the function of applied *dc* magnetizing field under *ac* magnetic field 5 Oe and frequency 1093 Hz is measured. The nanodimensions of NZF/BT are observed dielectric constant up to 120 MHz. The optical activity of NZF/BT nanostructures is shown by Fluorescence spectra. © *2014 AIP Publishing LLC*.
[http://dx.doi.org/10.1063/1.4896118]

I. INTRODUCTION

Multifunctionality of magnetoelectric (ME) multiferroic (MF) provides significant potentials for applications such as spintronics, memory, and sensors, to the next-generation multifunctional devices.[1–3] The reported work of MF shows small study for small size nanoparticles and one-dimensional (1D) nanostructures (nanorods, nanowires, etc.), resulting in improvement of ferroelectricity, ferromagnetism, and ME coefficient. Cai *et al.*[4] considered near-surface depolarizing effect, and the surface tension induced by 1D nanowires using first-principles calculation results in large enhancement of spontaneous polarization along the wire direction because the compressive stress induced by surface curvature would produce an effective tensile in the direction of length of nanowire. Generally, spontaneous polarization is caused by atomic off-center displacements resulting from a delicate balance between long-range Coulomb interaction and short-range covalent interaction.[5] In 1D MF nanostructures, long range interaction is truncated due to the lack of periodicity and short range one is significantly modified near the surface boundary.

The ME response is the appearance of magnetization that can be modified by an applied electric field, while the electric polarization can be tailored by applying a magnetic field has been served as an intrinsic effect at low temperature and high magnetic field in some single phase multiferroic systems.[6,7] Alternatively and with greater design flexibility, MF composites have been introduced, where a magnetostrictive phase is mechanically coupled to a piezoelectric phase, originating from the elastic interaction among the subsystems via stress mediation.[8] A large magnetoelectric output voltage has been observed in Pb based MF composites. But recently, owing to concerns regarding the environmental pollution and its toxicity to human beings,[9] Pb based MFs are prohibited. Therefore, extensive research is going on worldwide to find Pb free MF composites with high value of ME coefficient. The MF composite of ferroelectric, BaTiO$_3$ (BT), and ferrites has been recently found to exhibit large ME response at room temperature and low magnetic field.[1,8,10–12] The ME behavior is strongly dependent on their microstructure and coupling interaction across ferromagnetic-ferroelectric interface. Among various perovskite based MFs, the tetragonal phase of BT nanostructure rarely exists and resides stress near grain boundaries for enhancement of polarization.[13] The twinning behavior of polycrystals, which reduce the bulk strain energy, contributes to the resulting twin structure.[14] In the recent work,[15] we have reported large ferromagnetism in Ni$_{0.6}$Zn$_{0.4}$Fe$_2$O$_4$ ferrite nanostructure and therefore become a suitable candidate for MF composite.

The MF BT nanostructures (nanoparticles, nanowire, nanorods, etc.) prepared by different synthesizing routes are divided into two categories: First is by adjusting appropriate

a)Author to whom correspondence should be addressed. Electronic addresses: kuldeep0309@yahoo.co.in. and dkuldep.physics@gmail.com. Tel.: +91 9418941286.

stoichiometric ratio as well as concentration of polymer acting as surfactant, etc.[3,11,13] The second process is hydrothermal, which is surfactant free, and the size and shape of nanostructure depends on the adjustment of pH value, hydrolysis time, and temperature.[7,16]

In the present paper, we have prepared MF composite of $Ni_{0.6}Zn_{0.4}Fe_2O_4$-$BaTiO_3$ (NZF/BT) nanostructure by two different routes, i.e., chemical combustion and hydrothermal. The resulting structural, microstructural, ferroelectric, ferromagnetic, ME coefficient, dielectric, and optical properties have been investigated.

II. EXPERIMENTAL DETAILS

A. Chemical combustion synthesis of $Ni_{0.6}Zn_{0.4}Fe_2O_4$-$BaTiO_3$ (CNZF/BT) composite

The CNZF/BT precursor was prepared by mixing the magnetic NZF and ferroelectric BT phases together from nickel nitrate ($Ni(NO_3)_2.6H_2O$), zinc nitrate ($Zn(NO_3)_2.6H_2O$), ferric nitrate ($Fe(NO_3)_3.9H_2O$), barium nitrate ($Ba(NO_3)_2$), tetra-*n*-butyl orthotitanate ($C_{16}H_{36}O_4Ti$), polyethylene glycol (PEG), and urea taken in desired stoichiometric ratios. The process involves two steps: First, the nitrates of nickel, zinc, and iron were added to PEG and kept stirring at room temperature called solution A. Second, tetra-*n*-butyl orthotitanate was dissolved in ethanol, and then, barium nitrate was added and stirred at room temperature for homogenous mixing called solution B. Both the solution A and B were mixed dropwise with continuous stirring and raised the room temperature to $50\,°C$. Urea was added to it, and the temperature was then raised to $70\,°C$ till combustion takes place. Overall, possible chemical reaction is summarised in Fig. 1(a). All nitrates were acting as oxidising agents and PEG and urea were reducing agents. Brown powder so obtained was purified by washing with a mixture of ethanol and water (double distilled) and finally, subjected to annealing at $500\,°C$ for 5 h.

B. Hydrothermal synthesis of $Ni_{0.6}Zn_{0.4}Fe_2O_4$-$BaTiO_3$ (HNZF/BT) composite

The precursor of HNZF/BT composite mixed together from magnetic (NZF) and ferroelectric (BT) using nickel chloride ($NiCl_2.6H_2O$), zinc chloride ($ZnCl_2.6H_2O$), iron chloride ($FeCl_3$), barium acetate ($Ba(C_2H_5OO)_2$), tetra-*n*-butyl orthotitanate ($C_{16}H_{36}O_4Ti$), and KOH as the starting materials. These chlorides of nickel, zinc, and iron were dissolved in mixture of ethanol and distilled water and taken as

solution one. Tetra-*n*-butyl orthotitanate was dissolved in ethanol, and then, barium acetate was added to it and taken as solution two. Both of solutions were mixed and subjected to stirring at room temperature for homogenous mixing for 2 h at room temperature. The pH was adjusted to 13 by the addition of mineralizer KOH with stirring. The final solution was poured into Teflon lined steel autoclave, which was kept for heating in programmed furnace at $180\,°C$ for 48 h. The resultant material was washed several times with ethanol–water mixture for purification and then dried at $80\,°C$ for 8 h in an oven. A detailed of hydrothermal synthesis of NZF/BT is also given in Fig. 1(b).

C. Characterization

The crystalline structure was analyzed by X-ray diffraction (XRD) by using X'Pert PRO PANalytical system and microstructure by transmission electron microscopy (TEM) by using HITACHI H-7500. For electrical measurements, the NZF/BT crystalline powder prepared from both of the synthesis routes was pressed into pellets of thickness ~0.5 mm by the cold isostatic pressing method with a pressure of 5 bar for 10 min and then sintered at $1000\,°C$ for 5 h. There may be possibility in the morphology that the resulting specimens have slight growth in their dimensions of grains, which was already described and shown by SEM images in our previous work of $PbTiO_3$ and $BaTiO_3$ based MF systems.[3,17] Polarization under the influence of applied electric field was measured using a Radiant Technologies ferroelectric test system. Magnetization of the NZF/BT was measured at room temperature using Lakeshore 7304 vibrating sample magnetometer. The ME coupling coefficient was measured by the dynamic field method by a system built in-house. A buffer and high-pass filter circuit to reduce the background voltage noise are employed in the measurement set-up to detect the induced ME voltage across the sample thickness. The room temperature dielectric measurement was performed on CNZF/BT and HNZF/BT specimen with frequency varying from 20 Hz to 120 MHz using Precision Impedance analyzer (Wayne Kerr 6500B). The photoactivity is shown by fluorescence spectrum of the composite at room temperature using Edinburgh FLSP920 spectrofluorophotometer.
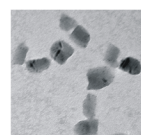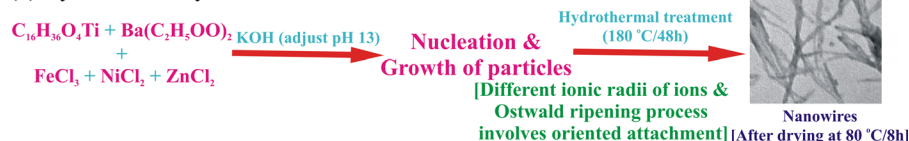
III. RESULTS AND DISCUSSION

The XRD patterns of both CNZF/BT and HNZF/BT composites revealed the presence of spinel and perovskite

(a) Chemical Combustion synthesis

$C_{16}H_{36}O_4Ti$ + $Ba(NO_3)_2$
+
$Fe(NO_3)_3$ + $Ni(NO_3)_2$ + $Zn(NO_3)_2$
[Oxidizing agents]

Stirring & heating (0 - 50 °C)
$H(OCH_2CH_2)_nOH$ + NH_2CONH_2
[Reducing agents]

→ **Dark brown Viscous gel**

Stirring & heating (50 ° - 70 °C)
Combustion

→ **Nanoparticles [After annealing at 500 °C]**

(b) Hydrothermal synthesis

$C_{16}H_{36}O_4Ti$ + $Ba(C_2H_5OO)_2$
+
$FeCl_3$ + $NiCl_2$ + $ZnCl_2$

KOH (adjust pH 13)

→ **Nucleation & Growth of particles [Different ionic radii of ions & Ostwald ripening process involves oriented attachment]**

Hydrothermal treatment (180 °C/48h)

→ **Nanowires [After drying at 80 °C/8h]**
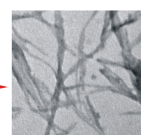
FIG. 1. Chemical combustion and hydrothermal synthesis routes, and growth mechanism of NZF/BT nanostructure.

FIG. 2. XRD pattern of CNZF/BT and HNZF/BT nanostructure.

phases together corresponding to NZF and BT, respectively, as shown in Fig. 2. The spinel phase of NZF shown by diffraction angle $2\theta = 3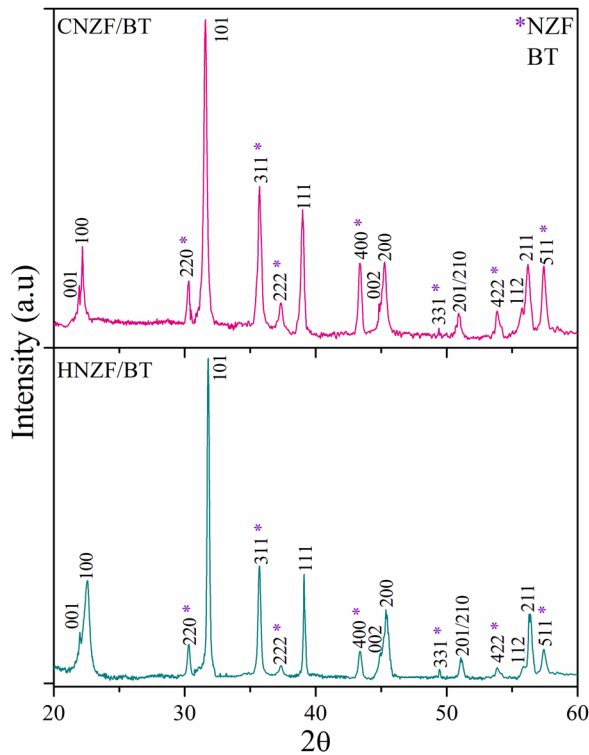0.18°$, $35.87°$, $37.33°$, $43.39°$, $49.45°$, $53.93°$, and $57.33°$ corresponds to (220), (311), (222), (400), (331), (422), and (511), respectively. While $2\theta = 21.93°$, $22.18°$, $31.51°$, $39.14°$, $44.97°$, $45.21°$, $50.91°$, $55.75°$, and $56.24°$ corresponds to (001), (100), (101), (111), (002), (200), (201/210), (112), and (211), respectively, indicating tetragonal polycrystalline phase of BT. The reflections 001/ 100 and 200/002 are the splitting of cubic into tetragonal phase. Using the CHEKCELL lattice constant refinement program, the lattice parameters of both phases are summarized in Table I. The distortion ratio c/a of tetragonal phase is 1.007 and 1.0083, respectively, for CNZF/BT and HNZF/ BT. The broadening of the full width at half maxima of the diffraction peaks indicates the formation of nanocrystalline products.

Figure 3 reveals the TEM images at different magnification of CNZF/BT and HNZF/BT composite. As shown in Fig. 3(a), the CNZF/BT consists of nanoparticles of very small size having cubic like faces of average diameter 4 nm.

However, Fig. 3(b) shows the nanowires like structure consisting of large number of nanowires. The observed average diameter of HNZF/BT wire is 3 nm, and the length is greater than 150 nm. The inset of Figs. 3(a′) and 3(b′) shows the random distribution of ferroelectric (BT) and magnetostrictive (NZF) phases into a single nanocrystal. This can be achieved by mixing ceramic precursors for each phase together, forming a blended MF solution. When combustion/hydrothermal/ calcination, such a solution will produce biphasic MF nanostructure with a random distribution of grains in each phase. Such type of distribution of MF phases is given in the recent reported work.[18]

Figures 1(a) and 1(b) show the possible growth mechanism for small nanoparticles of CNZF/BT and nanowires of HNZF/BT composite. In case of CNZF/BT [Fig. 1(a)], the chemical combustion was used where the nanofabrication temperature (annealing) is low (500 °C), resulting in small growth of grains. Generally, nitrates serve as excellent providers of oxidising environment, while the urea and PEG serve as reducing and chelating agents. PEG and urea gets chelation with metal ions. Formation of ammonium nitrate by the reaction of urea with metal nitrate ions helps in lowering of ignition temperature and provides combustion at low temperature with ease. PEG too gets chelated with metal ions and help in combustion process. As combustion takes place, flame release of gases like oxides of nitrogen and carbon dioxide, and water leads to shattering of material into nanosize product.

Figure 1(b) is the HNZF/BT composite showing the fabrication of nanowires by hydrothermal synthesis using ethanol as solvent. This solvent plays a key role to create various shapes because ethanol has such ability due to its high coordinating nature towards the metal cation. The main reason for the particles coarsening or Ostwald ripening process is the surface energy reduction.[19] This process involves formation of small crystalline nuclei in a suspension which is supersaturated, and then, it is followed by crystal growth, in which the bigger particles will grow at the cost of the smaller ones due to the energy difference between large and smaller particles. The hydrothermal synthesis leads to particle coalescence if treated for longer period of hydrolysis temperature (180 °C for 48 h), due to an increased number of coalescence occasions. Addition of KOH helps in precipitation of material and provides basic environment for the reaction. The role of oriented attachment in hydrothermal conditions is that under dispersed conditions, the anisotropic particles are formed by successive collisions without grain rotation and can lead to various particle shapes. The final

TABLE I. Values of lattice parameters a of NZF and BT (a and c), diameter (d), length (l), spontaneous polarization (P_s), saturation magnetization (M_s), maximum magnetoelectric coefficient (α_E), and dielectric constant (ε_r) of NZF/BT nanostructures.

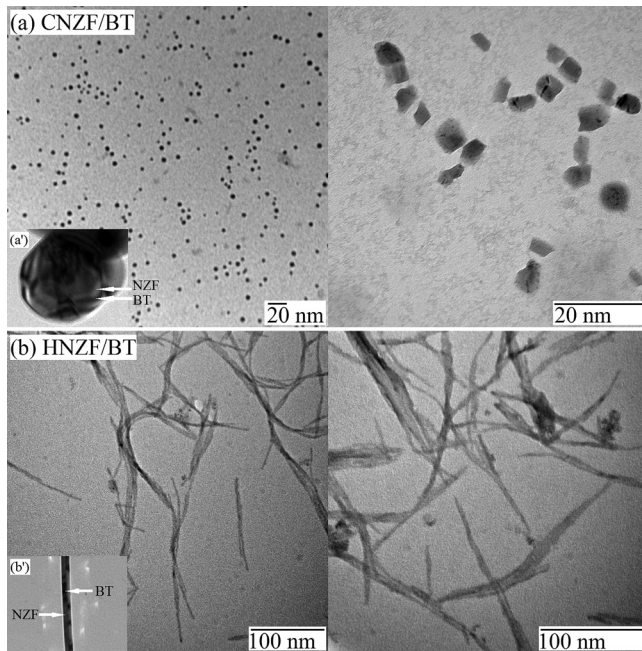| | Lattice constant | | | Multiferroic properties | | | | | |
| | NZF | BT | | | NZF/BT | | | | |
Sample	a (Å)	a (Å)	c (Å)	d (nm)	l (nm)	M_s (emu/g)	P_s (μC/cm^2)	α_E (mV/cm Oe)	ε_r (10 MHz)
CNZF/BT	8.395	3.995	4.023	4	…	12.26	16.51	78.57	31
HNZF/BT	8.441	3.998	4.031	3	>150	18.35	24.37	102.54	55

FIG. 3. TEM images of CNZF/BT and HNZF/BT nanostructure. Insets ((a′) and (b′)) show random distribution of NZF and BT phases.

particle can result from several attachment events along the same surface, giving an uncontrollable shape in agglomerates. It is believed that the present case involves under dispersed conditions; the steric hindrance may have led to effective collisions in only one crystallographic direction due to different ionic radii of all metal ions resulting into formation of nanowires like structure.[7]

Figures 4, 5(a), and 5(b) show the coexistence of ferroelectricity and ferromagnetism of CNZF/BT and HNZF/BT nanostructure, respectively, by measuring polarization versus electric field (*P-E*) and magnetization versus magnetizing field (*M-H*) hysteresis curves at room temperature. The *P-E* hysteresis loops measured at room temperature on poled specimen of CNZF/BT composite with 50 Hz frequency of polarization [Fig. 4(a)] results in the value of spontaneous
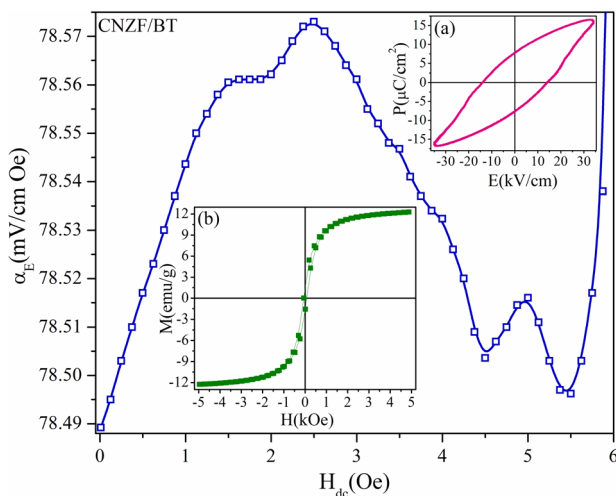

FIG. 4. ME voltage coefficient (α_E) with H_{dc} under the influence of $H_{ac} = 5$ Oe and frequency of 1093 Hz of CNZF/BT nanoparticles. Insets show (a) *P-E* and (b) *M-H* hysteresis.

FIG. 5. ME voltage coefficient (α_E) with H_{dc} under the influence of $H_{ac} = 5$ Oe and frequency of 1093 Hz of HNZF/BT nanowires. Insets show (a) *P-E* and (b) *M-H* hysteresis.
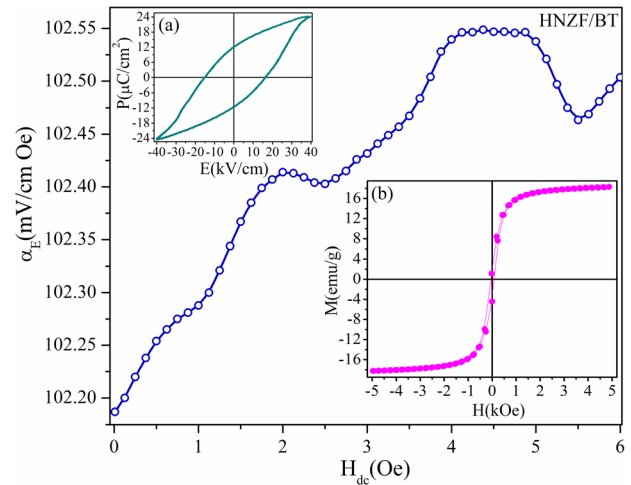
polarization, $P_s = 16.51\,\mu C/cm^2$, remanent polarization, $P_r = 7.54\,\mu C/cm^2$, and coercive field, $E_c = 13.97\,kV/cm$. However, the values of $P_s = 24.37\,\mu C/cm^2$, $P_r = 11.78\,\mu C/cm^2$, and $E_c = 15.54\,kV/cm$ are observed in HNZF/BT composite [Fig. 5(a)]. These values of P_r for both the samples of NZF/BT composite are given in Table I and shows improvement than reported work of BT based composites,[2,12,20,21] which are explained as: first; the surface defects by large value of surface to volume ratio of nanostructures. Second, the polycrystalline phase of BT is tetragonal. This tetragonal phase with nanograins has twin structure by which the stress residing near grain boundaries can easily control depolarization field, and therefore, the long-range interactions support the development of homogeneous polarization; and the elastic constraints form strain energetic and its stress relieving twinning mechanism. Hence, the enhancement in ferroelectric polarization[14] is possible. Third is the epitaxial strain growth between ferrite and ferroelectric interface introduced by the lattice mismatch between cubic phase of spinel (NZF) and tetragonal (BT) result in large ferroelectric polarization.[22] It has also been observed that the NZF/BT composite prepared by hydrothermal synthesis have higher value of polarization than those by chemical combustion, which is explained based on the shape of nanostructure. The HNZF/BT composite has 1D nanowire like structure and the ferroelectric polarization in such type of 1D system is explained on the basis of First-principles density functional theory using local density approximation Hellmann-Feynman theorem by Cai *et al.*[4] for their ferroelectric system of perovskite $PbTiO_3$ nanowires. By this assumption, the surface compressive stress caused by 1D shape produces an effective tensile in the length direction in nanowires and then leads to a big off-center displacements that enhances the spontaneous polarization. This enhancement in polarization is attributed to the competition between itself surface tension and near-surface depolarizing effect.

Figures 4 and 5(b) show the ferromagnetic behaviors of NZF/BT composites by measuring *M-H* hysteresis at room temperature. The values of saturation magnetization (M_s) are

12.26 and 18.35 emu/g, and coercive field (H_c) are 81.93 and 69.56 Oe, respectively, for CNZF/BT and HNZF/BT nanostructure, and are also given in Table I. In both of these composites of NZF/BT, the nanostructural grains show ordered magnetic structure (soft ferromagnetic) causing a non-linear hysteric character because the large surface to volume ratio of nanograins leads to superficial spin canting, spin pinning, or broken exchange bonds.[23] It is possible from microstructure that the area of NZF nanograins are percolated by a large number of small BT particles, causing an increasing number of disordered regions at the interface, and therefore, the magnetic properties of NZF/BT nanocomposite are determined not only by the NZF concentration but also by the degree of connectivity of the two-phase component grains. The HNZF/BT shows nanowire like structure resulting in higher magnetization than CNZF/BT nanoparticles. This is explained by the effective exchange interactions between the unpaired electrons spins, originating from the surface defects such as oxygen vacancy clusters instead of single neutral oxygen vacancies associated with the nanoparticles.[13]

Multiferroicity is the coexistence of ferroelectricity and ferromagnetism gives ME coupling whose strength is measured in terms of magnetoelectric coefficient (α_E) under a static magnetic field H_{dc}, superimposed with a small *ac* magnetic field H_{ac}. The α_E is given by $\alpha_E = V_{out}/H_{ac} \times t$, where t is the sample thickness and V_{out} is the induced ME voltage. The variations of α_E with H_{dc} at *ac* magnetic field frequency of 1093 Hz and *ac* magnetizing field of 5 Oe for both the composites of NZF/BT nanostructure measured at room temperature are shown in Figs. 4 and 5. The maximum value of α_E is 78.57 and 102.54 mV/cm Oe, respectively, for CNZF/BT and HNZF/BT. These values of α_E are given in Table I and show improvement than the reported work of BT based composites.[7,12,13,24–32] Generally, the value of α_E linearly increases to a maximum value and then deceases linearly to zero with varying H_{dc} of applied magnetic field. But, in the present case of NZF/BT, the α_E is nonlinearly varying and also observe stability at certain value of applied H_{dc} magnetic field depends on two factors: first, the two-phase nanostructural composite coupled by interfacial strain where ME behavior is strongly dependent on their nanograins and the coupling interaction across the piezoelectric/magnetostrictive interface.[33] It is expected that a residual stress generated can be responsible for the eventual nucleation, evolution, and coalescence of voids, which strongly hinder the domain reorientation, and therefore control the resulting polarization of ME. Second, the dependence of magnetoelectric yield on the bias field, H_{dc}, may be ascribed to the nonlinear magneto-stress coupling because it is believed that a bias field favors a parallel spin alignment for all magnetic domains so that the magnetostrictive response is more significant.[33]

Figure 6 shows the variation of dielectric constant (ε_r) and dielectric loss (tan δ) of CNZF/BT and HNZF/BT nanocomposites measured at room temperature in the frequency range of 20 Hz–120 MHz. Both of the composites showing variation in the dielectric constant in the low frequency region is explained on the basis of space charge polarization due to inhomogeneous dielectric structure. These inhomogeneities exist due to impurities, porosity, and grain structure.[34]
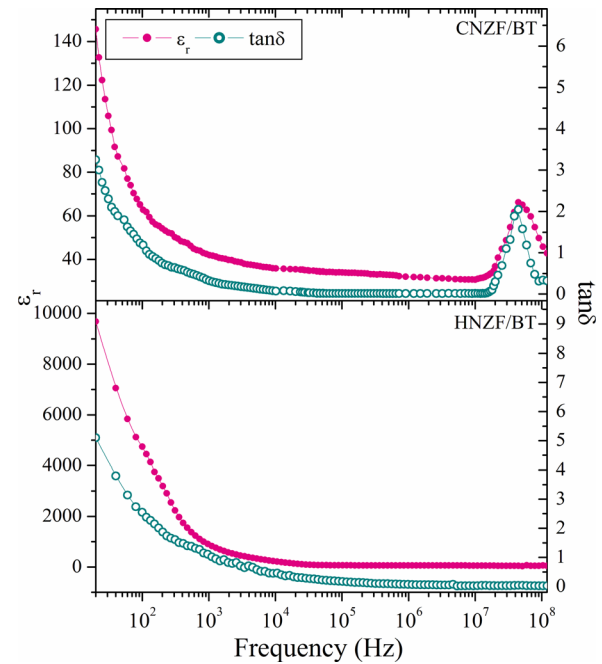

FIG. 6. Frequency dependent relative permittivity (ε_r) and loss (tan δ) of CNZF/BT and HNZF/BT.

The value of ε_r at 10 MHz is 31 and 55, respectively, for CNZF/BT and HNZF/BT. The composite CNZF/BT shows a resonance peak in both ε_r and tan δ near 45 MHz, which may arise from the matching between the frequency of the mobility of charge carrier and that of the applied electric field. While HNZF/BT has no such type of behavior up to 120 MHz is explained on the basis of different type of nanostructural formation in both of the composites. A slight decrease in ε_r and tan δ with the increase of frequency
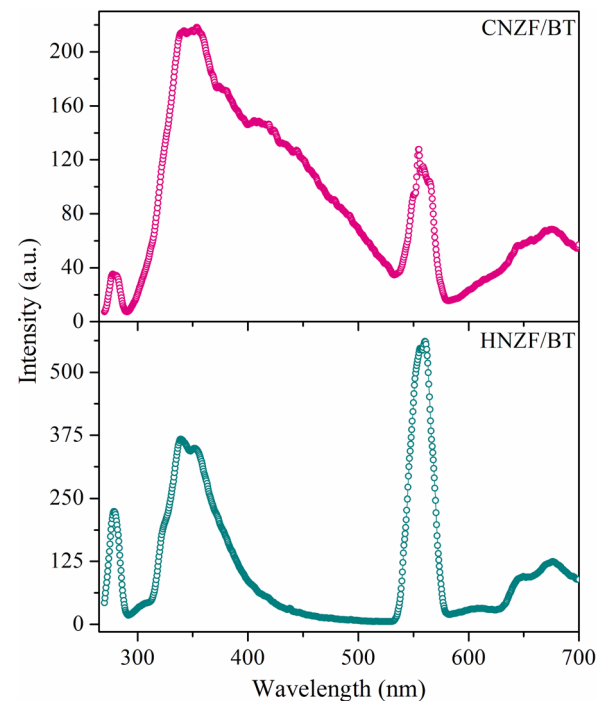

FIG. 7. Fluorescence spectra of CNZF/BT and HNZF/BT measured at room temperature.

indicates dielectric dispersion following the Maxwell-Wagner type interfacial polarization.[35,36]

Figure 7 shows fluorescence spectrum of NZF/BT nanocomposites at room temperature. It is well known that the point defects, oxygen vacancies, and interstitials are key factors responsible for emission spectrum. In case of BT, the charge transfer spectra from the central Ti^{3+} ion to a neighbouring O^{2-} ion inside octahedron of TiO_6^{8-} from intrinsic defects result into luminescence in the BT system.[37] While in case of NZF ferrite, first blue band observed is due to interstitial and defect emission, while system corresponding second band is due to their phase formation.[38] Composite HNZF/BT via hydrothermal synthesis shows remarkable high intensity of blue, green, yellow, and red band emissions than CNZF/BT.

IV. CONCLUSION

The MF NZF/BT composite has been successfully synthesized by chemical combustion and hydrothermal routes. The growth mechanism in the formation of small nanoparticles of CNZF/BT is given by the use of nitrates as oxidising agent, and PEG and urea as reducing agent during combustion and annealing. The nanowires of HNZF/BT are formed due to different ionic radii of metal ions, and Ostwald ripening process involves oriented attachment during hydrothermal treatment. The XRD results show the formation of spinel cubic phase of NZF and tetragonal polycrystalline phase of BT. The TEM images show that the average particles size is 4 nm for CNZF/BT, and for HNZF/BT nanowires, the average diameter is 3 nm and length is >150 nm. The value of $P_s = 16.51$ and $24.37 \, \mu C/cm^2$, and $P_r = 7.54$ and $11.78 \, \mu C/cm^2$, and $E_c = 13.97$ and $15.54 \, kV/cm$, respectively, observed for CNZF/BT and HNZF/BT. The values of M_s are 12.26 and 18.35 emu/g, respectively, measured for CNZF/BT and HNZF/BT. The maximum value of α_E is 78.57 and 102.54 mV/cm Oe, respectively, observed for CNZF/BT and HNZF/BT MFs. The value of ε_r at 10 MHz is 31 and 55, respectively, measured for CNZF/BT and HNZF/BT. The point defects, oxygen vacancies, and interstitials give the emission spectrum of NZF/BT nanostructure.

[1]C. S. Antoniak, D. Schmitz, P. Borisov, F. M. F. Groot, A. Stienen, A. Warland, B. Krumme, R. Feyerherm, E. Dudzik, W. Kleemann, and H. Wende, Nat. Commun. **4**, 2051 (2013).
[2]B. Li, C. Wang, and G. Dou, CrystEngComm **15**, 2147 (2013).
[3]K. C. Verma, R. K. Kotnala, and N. S. Negi, Appl. Phys. Lett. **92**, 152902 (2008).
[4]M. Q. Cai, Y. Zheng, B. Wang, and G. W. Yang, Appl. Phys. Lett. **95**, 232901 (2009).
[5]R. E. Cohen, Nature (London) **358**, 136 (1992).
[6]T. Kimura, T. Goto, H. Shintani, K. Ishizaka, T. Arima, and Y. Tokura, Nature **426**, 55 (2003).
[7]K. C. Verma, V. Gupta, J. Kaur, and R. K. Kotnala, J. Alloys Compd. **578**, 5 (2013).
[8]G. Liu, C. W. Nan, Z. K. Xu, and H. Chen, J. Phys. D: Appl. Phys. **38**, 2321 (2005).
[9]Y. Jia, S. W. Or, J. Wang, H. L. W. Chan, X. Zhao, and H. Luo, J. Appl. Phys. **101**, 104103 (2007).
[10]H. Wu, B. Xu, A. Liu, and G. Chai, J. Phys. D: Appl. Phys. **45**, 455306 (2012).
[11]K. C. Verma and R. K. Kotnala, Solid State Commun. **151**, 920 (2011).
[12]K. Sadhana, S. R. Murthy, S. Jie, Y. Xie, Y. Liu, Q. Zhan, and R. W. Li, J. Appl. Phys. **113**, 17C731 (2013).
[13]K. C. Verma, J. Kaur, N. S. Negi, and R. K. Kotnala, Solid State Commun. **178**, 11 (2014).
[14]M. H. Frey and D. A. Payne, Phys. Rev. B **54**, 3158 (1996).
[15]S. Singh, M. Singh, R. K. Kotnala, and K. C. Verma, Indian J. Pure Appl. Phys. **52**, 550–555 (2014).
[16]J. P. Zhou, L. Lv, Q. Liu, Y. X. Zhang, and P. Liu, Sci. Technol. Adv. Mater. **13**, 045001 (2012).
[17]J. Kaur, R. K. Kotnala, and K. C. Verma, Mater. Lett. **65**, 3160 (2011).
[18]G. Sreenivasulu, M. Popov, F. A. Chavez, S. L. Hamilton, P. R. Lehto, and G. Srinivasan, Appl. Phys. Lett. **104**, 052901 (2014).
[19]W. F. Ostwald, Phys. Chem. **22**, 289–302 (1897).
[20]T. Li, F. Zhang, H. Fang, K. Li, and F. Yu, J. Alloys. Compd. **560**, 167 (2013).
[21]J. Majeed, O. D. Jayakumar, H. G. Salunke, B. P. Mandal, G. Lawes, R. Naik, and A. K. Tyagi, RSC Adv. **3**, 596 (2013).
[22]C. Ederer and N. A. Spaldin, Phys. Rev. Lett. **95**, 257601 (2005).
[23]B. Van den, D. R. Terrell, R. A. J. Born, and H. F. J. Giller, J. Mater. Sci. **9**, 1705 (1974).
[24]J. Shah and R. K. Kotnala, J. Mater. Chem. A **1**, 8601 (2013).
[25]T. X. Li, M. Zhang, F. J. Yu, Z. Hu, K. S. Li, D. B. Yu, and H. Yan, J. Phys. D: Appl. Phys. **45**, 085002 (2012).
[26]M. Lorenz, V. Lazenka, P. Schwinkendorf, F. Bern, M. Ziese, H. Modarresi, A. Volodin, M. J. V. Bael, K. Ziese, A. Vantomme, and M. Grundmann, J. Phys. D: Appl. Phys. **47**, 135303 (2014).
[27]E. V. Ramana, F. Figueiras, M. P. F. Graca, and M. A. Valente, Dalton Trans. **43**, 9934 (2014).
[28]Y. Shen, J. Sun, L. Li, Y. Yao, C. Zhou, R. Su, and Y. Yang, J. Mater. Chem. C **2**, 2545 (2014).
[29]R. F. Zhang, C. Y. Deng, L. Ren, Z. Li, and J. P. Zhou, Mater. Res. Bull. **48**, 4100 (2013).
[30]A. Gupta and R. Chatterjee, J. Eur. Ceram. Soc. **33**, 1017 (2013).
[31]R. C. Kambale, K. M. Song, and N. Hur, Curr. Appl. Phys. **13**, 562 (2013).
[32]C. Nayek, K. K. Sahoo, and P. Murugavel, Mater. Res. Bull. **48**, 1308 (2013).
[33]C. Brosseau, V. Castel, and M. Potel, J. Appl. Phys. **108**, 024306 (2010).
[34]M. A. E. Hiti, J. Magn. Magn. Mater. **164**, 187 (1996).
[35]J. C. Maxwell, *Electricity and Magnetism* (Oxford University Press, London, 1973).
[36]K. W. Wagner, "Electricity and magnetism," Ann. Phys. **40**, 817 (1913).
[37]J. Yu, L. Yue, S. Liu, B. Huang, and X. Zhang, J. Colloid Interface Sci. **334**, 58–64 (2009).
[38]C. H. Chen, Y. H. Liyang, and W. D. Zhang, J. Alloys Compd. **501**, 168 (2010).